Ultraviolet Raman spectroscopy of N 2 in a recombining atmospheric pressure plasma

Sean Mcguire, C Tibère-Inglesse, C. Laux

Ultraviolet Raman spectroscopy of N_2 in a recombining atmospheric pressure plasma

S. D. McGuire, A. C. Tibère-Inglesse and C. O. Laux

Laboratoire EM2C, CNRS UPR288, CentraleSupélec, University Paris-Saclay, 10 rue Joliot-Curie, 91190, Gif-sur-Yvette, France

E-mail: [1]sean.mc-guire@centralesupelec.fr

Abstract. We report ultraviolet spontaneous Raman scattering measurements of temperature in a recombining nitrogen plasma. The plasma source is an atmospheric pressure RF torch facility. A N_2/Ar mixture is injected into the torch and heated to approximately 6800 K at the torch exit. Raman scattering measurements are in agreement with optical emission spectroscopy measurements of temperature at the torch exit. A 15-cm water-cooled tube is then mounted at the torch exit to rapidly cool the gas and produce a recombining plasma. Raman scattering measurements indicate a temperature of approximately 3300 K at the tube exit, significantly lower than previous emission spectroscopy estimates. The Raman measurements were confirmed via separate Rayleigh scattering measurements. The lack of agreement between the emission spectroscopy, which only yields information on excited states, and Raman scattering measurements shows that the plasma is far from equilibrium at the exit of the recombining tube. These experiments provide a basis for studying recombining plasmas which, among other applications, are important for atmospheric reentry applications and plasma processing.

1. Introduction

We present ultraviolet vibrational Raman scattering measurements of N_2 X $^1\Sigma_g^+$ density and temperature in a recombining N_2/Ar plasma. This plasma is produced using an atmospheric pressure plasma torch facility. It is then passed through a water-cooled brass tube in order to rapidly cool the plasma and force it out of chemical equilibrium. The facility permits measurements of recombination kinetics and provides a simple experimental model for thermal and chemical kinetic phenomena encountered during atmospheric reentry. Such recombination phenomena are predicted to have a strong impact on afterbody heating, which becomes important at higher entry velocities.[1, 2] At the inlet to the water-cooled tube, the temperature is measured to be 6800 K and the plasma is, by all measures, in equilibrium.[3] Previously, Gessman and Laux et al [4, 5, 6, 7, 8] studied the recombining plasma at the exit of the water-cooled tube using emission spectroscopy and reported non-equilibrium vibrational population distributions in several excited states of N_2 as well as measurements of the rotational temperature using optical emission spectroscopy (OES).

We return to this experiment with new molecular nitrogen ground state temperature measurements obtained by Raman scattering for comparison with their previous emission measurements.

Vibrational Raman scattering has seen widespread use in the combustion community as documented by Eckbreth.[9] It has also been used in pulsed nanosecond discharges where non-equilibrium population distributions occur.[10, 11, 12, 13] Within the hypersonic research community, it has been used in several shock tube facilities to attain measurements of vibrational population distributions.[14, 15, 16] Studer and Vervisch performed spontaneous Raman scattering measurements of N_2 and O_2 in the boundary layer of a high enthalpy air flow over a cold flat plate.[17] They reported measurements of vibrational temperature, rotational temperature and density in the free stream and throughout the boundary layer. The measurements reported in this paper use a similar approach, but a different experimental configuration: a N_2/Ar mixture is used rather than air in order to isolate nitrogen chemical kinetics; the plasma at the entrance to the tube is in thermal equilibrium as a result of a higher operating pressure; and a water-cooled tube, rather than a flat plate, is used to rapidly cool the gas. Though simple, vibrational Raman scattering is a very weak process and often requires effort to both increase signal and decrease noise under realistic operating conditions. One approach for increasing signal is to operate in the ultraviolet region of the spectrum, where Raman cross-sections increase substantially, leading to larger signals.[9] This approach avoids more complicated experimental configurations such as multi-pass cells or nonlinear CARS. We use a frequency-doubled dye laser in order to perform ultraviolet vibrational Raman scattering measurements of both vibrational temperature and molecular nitrogen density in the ground state. Knowledge of these populations is important given that the bulk of molecular nitrogen is in the ground state. The Raman scattering technique also provides a separate measure of rotational temperature for comparison with the previous emission measurements. We find that these Raman scattering measurements yield a much lower temperature than the emission measurements at the exit of the water-cooled tube.

2. Experimental Setup

The plasma torch facility used to produce the plasma at the inlet of the water-cooled test-section is a TAFA Model 66 inductively coupled plasma (ICP) torch powered by a 120 kVA radio frequency LEPEL Model T-50-3 power supply. The power supply operates at 4 MHz and can supply a maximum of 12 kV DC and 7.5 A to the oscillator plates. Details of the plasma torch facility are provided in previous publications: for example, see MacDonald et al.[18, 19, 20] For the experiments presented here, a 1-cm diameter exit nozzle was used. Figure 1 shows a schematic of the facility which includes radial, axial and swirl injectors. Calibrated flow meters are used to control the mass flow rate of each gas through the system. A N_2/Ar gas mixture was used for these measurements. The flowrate was 1.5 g/s (50 slpm) for argon and 1.9 g/s (90 slpm) for N_2. 75% of the Argon was injected via the swirl injectors and 25% via the axial injectors. All of the N_2 was injected through the radial injectors. Directly at the exit of the torch, which corresponds to the inlet of the water-cooled test-section, temperature measurements could be obtained by measuring the absolute emission from lines of atomic nitrogen and argon. The procedure for

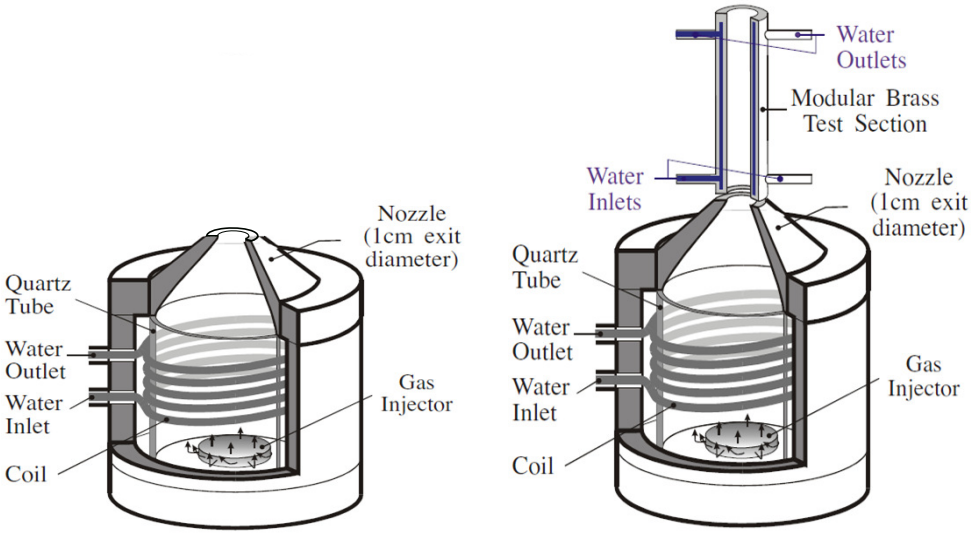

Figure 1. *Left*: Schematic of the plasma torch facility showing the head and nozzle assembly. The plasma is at equilibrium and, for the N_2/Ar mixture used, is at a temperature of about 6800 K at the nozzle exit. *Right*: A brass water-cooled tube, 15 cm in length, can be used to rapidly cool the plasma and leave it in a state of chemical non-equilibrium.

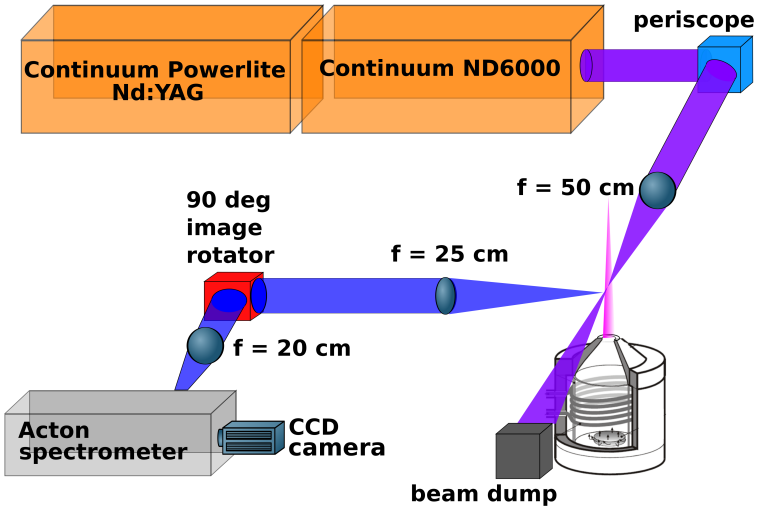

Figure 2. Experimental setup for Raman scattering measurements. The periscope consists of two quartz prisms for adjusting the height and direction of the laser beam.

emission measurements is documented in Refs. [3, 7, 21].

The water-cooled tube forces the plasma to recombine rapidly, leaving it in a state of chemical non-equilibrium. Figure 1 shows the water-cooled tube mounted at the torch exit. The tube, made of brass, has an inner diameter of 1 cm and is 15 cm in length. The average velocity of the plasma

at the inlet to the water-cooled tube is estimated to be approximately 500 m/s at the tube inlet‡ and thus the time to transit the tube is $\approx 300\mu s$. Based on this velocity and the temperature profile, the total enthalpy per unit time passing the exit of the torch is estimated at 19 kW. At the exit of the water-cooled tube, the gas temperature has decreased to a level where emission from atomic nitrogen and argon is no longer detectable and, therefore, could not be used to estimate the temperature for comparison with the Raman measurements. However, the temperature was measured from N_2^+ rotational lines as described in Ref. [6].

For Raman measurements, a frequency doubled Continuum dye laser was used to generate a 10 ns, 30 mJ ultraviolet pulse at 281 nm. Rhodamine 590 dye was used to supply a laser beam at 562 nm which was then frequency doubled to produce the final output at 281 nm. While the quadrupled output of a Nd:YAG laser at 266 nm may have sufficed for the measurements, the ability to tune the dye laser offered the ability to avoid potential laser-induced interferences in the UV. The wavelength used for these measurements, namely 281 nm, represented a compromise between avoiding laser-induced interferences and maximizing laser power. The laser output at 281 nm was focused onto the exit of the torch at the point of interest via a 50 cm CaF_2 lens (Fig. 2). The laser was polarized vertically and scattered light was collected at a right angle to the laser propagation axis. For imaging, two quartz lenses were used in conjunction with a 90° image rotator in order to image the spectrometer slit parallel to the laser axis (Fig. 3). The optical magnification from measurement point to camera was approximately 0.8. The spectrometer was a Princeton Instruments SP500 spectrometer with a UV enhanced Princeton Instruments PI-MAX 1 intensified camera mounted at the exit port. The grating was blazed at 240 nm and has 2400 grooves/mm. Slit widths between 100 and 300 μm were used for experiments. The instrumental function was determined by measuring the Rayleigh scattering profile centered on the laser wavelength. For every Raman measurement, a corresponding Rayleigh line profile was measured to determine the instrumental broadening. Figure 4 shows a measured Rayleigh scattering profile obtained for a slit width of 100 μm. The choice of slit depended on signal-to-noise ratio considerations: smaller slit widths result in less signal but higher resolution spectra for more accurate determination of temperature. Though the measured instrumental functions are not trapezoidal, it is useful for the theoretical discussion that follows to approximate them as trapezoidal and to find the equivalent FWHM. A slit width of 100 μm corresponds approximately to a trapezoidal instrumental function with a FWHM of 0.04 nm. Slit widths of 200 μm and 300 μm correspond to trapezoidal instrumental functions with FWHM of 0.08 and 0.10 nm, respectively. Note that these trapezoidal instrumental functions are not used in the final analysis: rather, the measured Rayleigh signal is used to provide a measure of the exact instrumental function.

For imaging the scattered light, the PI-MAX camera was used in gate mode (gate width of 20 ns) with maximum intensifier gain. Measurements were taken over a 4 mm spatial window and pixel binning was used to produce a measured spectrum. Spectral collection could be accomplished

‡ The Prandtl number directly at the torch exit of the N_2/Ar mixture is approximately 0.7. If $Pr \approx 1$, the speed and temperature profiles may be assumed to be self-similar. This, together with conservation of mass and the fact that the plasma is in equilibrium allow for the calculation of a velocity profile.

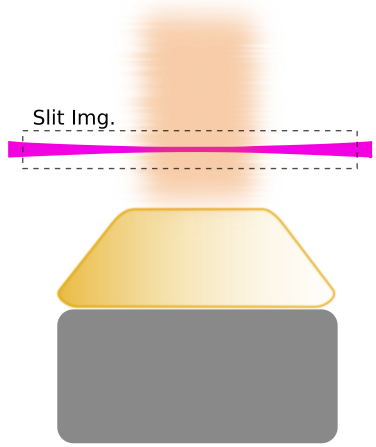

Figure 3. Relative positions of the laser focus, imaged spectrometer slit and torch nozzle. The laser is focused approximately 5 mm above the torch nozzle exit.

by varying the number of accumulations on CCD, by simply averaging several spectra to reduce noise or by some combination of these two. Increasing the number of accumulations on CCD resulted in an increase in signal, but also noise. Averaging individual spectra reduced the amount of noise but did not increase the signal. To maximize signal-to-noise, we found that averaging 50 individual spectra, each obtained by accumulating 100 images on the CCD yielded the best result. The total time to obtain a single spectrum was then approximately 8 minutes. Note that these measurements were not synchronized to the RF voltage/current used to generate the plasma in the ICP torch. The plasma properties at the torch exit were viewed as steady: an assumption justified by the stable emission measurements which have been previously made in this facility.[3] Minimal interference from laser-induced fluorescence and from torch emission was observed at wavelengths close to the Stokes signal, but were not observed to overlap the signal itself. This interference was attributed to the nitrogen second positive system and was observed only at the torch exit, which corresponds to the water-cooled tube inlet. No fluorescence was observed at the exit of the water-cooled tube. Background spectra were taken by blocking the laser and recording spectra. These background spectra were then subtracted from the signal obtained with the laser to produce a final Raman spectrum. Both anti-Stokes and Stokes signals were observed. However, only the Stokes signal was used for analysis because it was stronger and because the camera efficiency was better at the Stokes wavelength.

3. Theory

3.1. Raman model

For temperature measurements, the spectral profile of the Raman signal was fitted with a theoretical model. Only Q-branch rotational transitions ($\Delta J = 0$) were accounted for, as these are much

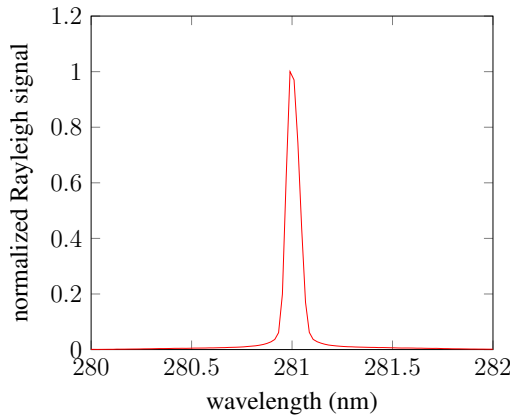

Figure 4. Normalized Rayleigh spectrum obtained for a spectrometer slit width of 100 μm. This spectrum was taken in ambient air (300 K, 1 atm).

stronger than the O- and S- rotational branches ($\Delta J = \pm 2$). Furthermore, for the Q-branch transitions, the anisotropy contribution was ignored as it is much weaker than the mean of the polarizability tensor. This removed any dependence of the Raman cross-section on rotational level. Given these assumptions, the relative intensity of the Stokes-shifted Raman transition at frequency $\omega_{laser} + \Delta\omega$ was taken to be:

$$\mathcal{I}(\omega_{laser} + \Delta\omega) = N_{\nu J}\ (\nu + 1) \tag{1}$$

where ν and J represent the vibrational and rotational quantum numbers of the initial state. $\Delta\omega$ is the Raman shift corresponding to $\Delta\nu = 1$ and $\Delta J = 0$. $N_{\nu J}$ is the fractional population of N_2 in the initial state corresponding to vibrational level ν and rotational level J: this includes the relevant Boltzmann factor, rotational degeneracy and nuclear spin degeneracy for the particular state. Note the dependence on the vibrational level expressed by the factor $(\nu + 1)$ which arises from the Raman cross-section. After applying this equation across all populated levels of N_2, the resulting intensity profile was convolved with the appropriate instrumental function. As an input, the model accepts both vibrational and rotational temperatures. For temperature analysis, both the theoretical and experimental spectra were normalized. A fitting routine then minimized the residual between the experimental and theoretical curves to produce a final estimate of the vibrational and rotational temperatures.

Figure 5 shows three normalized theoretical Raman spectra, one at $T_{vib} = T_{rot} = 300$ K, a second at $T_{vib} = T_{rot} = 3000$ K and another at $T_{vib} = T_{rot} = 7000$ K. The different vibrational transitions are highlighted in the figure and illustrate the dependence of the spectrum on vibrational temperature. The rotational temperature impacts the shape of each vibrational feature, and is thus also a parameter that can be inferred from the Raman spectrum. This provides an estimate of the translational temperature given the fast equilibration between rotation and translation in ground state N_2 at atmospheric pressure[7].

For density measurements, the absolute magnitude of the signal was measured relative to Raman scattering from room temperature air. The total area under the Raman spectrum depends

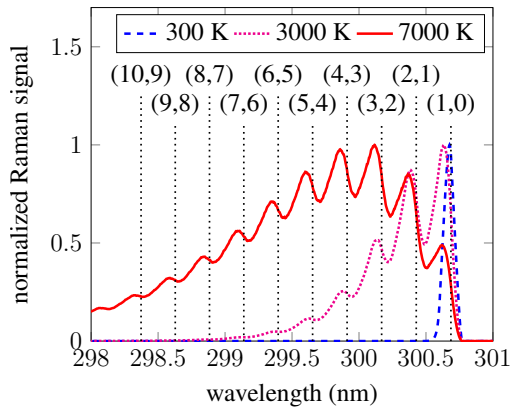

Figure 5. Modeled Raman spectra for $T_{vib} = T_{rot} = 300$ K, $T_{vib} = T_{rot} = 3000$ K and $T_{vib} = T_{rot} = 7000$ K. The instrumental function used here was triangular with FWHM = 0.08 nm, which closely approximates the instrumental function when using a slit width of 200 μm. Each spectrum has been normalized to its maximum. The vertical dotted lines and labels identify the various vibrational bands (ν',ν''), where ν' and ν'' represent the vibrational quantum numbers of the upper and lower states, respectively.

linearly on the density, but also on the vibrational temperature. This temperature dependence is a result of the dependence of the scattered intensity on the vibrational level (Eqn. 1). The total area can thus be written as follows: $\mathcal{A} = \left(N_{N2}/N_{N2}^{ref}\right) F(T, N_{N2}^{ref})$, where N_{N2} is the total density of N_2. $F(T, N_{N2}^{ref})$ represents the area under the Raman curve calculated at vibrational temperature T and at reference density N_{N2}^{ref}. The $\mathcal{A}$ parameter was measured both in the plasma and in room temperature air. Then, by setting $N_{N2}^{ref} = 1$, the ratio of these areas could be used to determine the density in the plasma as follows:

$$\frac{\mathcal{A}_{plasma}}{\mathcal{A}_{air}} = \frac{N_{plasma}\, F(T_{plasma}, 1)}{N_{air}\, F(T_{air}, 1)} \tag{2}$$

where $T_{air} = 300$ K and N_{air}, the density of N_2 in ambient air, are known. T_{plasma} is determined from the theoretical fit to the normalized experimental spectra. N_{plasma}, the density of N_2 in the plasma, is the only remaining unknown in Eqn. 2. It can thus be determined directly from Eqn. 2.

3.2. Fitting routine and error analysis

For temperature measurements, a fitting routine was used to minimize the residual between the normalized experimental and theoretical spectra for various temperatures. Before fitting, any background offset was first subtracted and the experimental spectrum then normalized to its maximum value. Note that this maximum value includes the experimental noise intrinsic to the measurement. For low signal-to-noise situations, the normalization can be biased by this noise. To avoid this bias, an amplitude scaling factor was also varied within the fitting routine and used to scale the experimental spectra to obtain the best fit. The fitting residual is given by:

$$\mathcal{R} = \frac{\sqrt{\sum_{\lambda_i} \left[E(\lambda_i) - T(\lambda_i)\right]^2}}{\sqrt{\sum_{\lambda_i} E(\lambda_i)^2}} \tag{3}$$

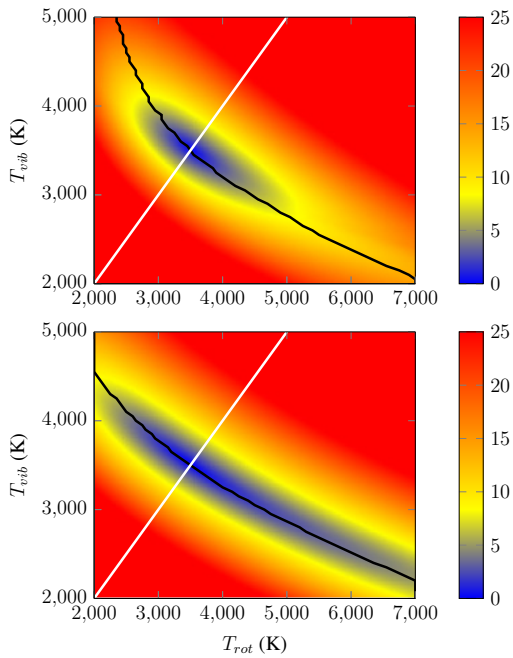

Figure 6. Residual contours (in %) showing the residual of a fit between a theoretical spectrum generated at (T_{rot},T_{vib}) and a theoretical spectrum generated for $T_{vib} = T_{rot} = 3500$ K. In all cases, the white line denotes equilibrium temperature coordinates $T_{rot} = T_{vib}$. For each rotational temperature, the black line denotes the corresponding vibrational temperature where the minimum residual was achieved. The absolute minimal residual is achieved for $T_{rot} = T_{vib} = 3500$ K as expected. *Top*: Trapezoidal instrumental function with a FWHM of 0.04 nm, which corresponds to a spectrometer slit width of 100 μm. *Bottom*: Trapezoidal instrumental function with a FWHM of 0.10 nm, which corresponds to a spectrometer slit width of 300 μm.

where $T(\lambda_i)$ and $E(\lambda_i)$ denote the theoretical and experimental values of the spectra at the wavelength λ_i, respectively. This dimensionless residual represents the total error as a percentage of the total signal.

Under non-equilibrium conditions, there can exist a large uncertainty in vibrational and/or rotational temperature. To illustrate, a normalized theoretical curve was generated for $T_{vib} = T_{rot} = 3500$ K. Next, the fitting routine was used to calculate the residual between this normalized spectrum and normalized spectra generated for various other combinations of T_{vib} and T_{rot}. For this test case, no artificial noise was added and thus the best fit is necessarily for $T_{vib} = T_{rot} = 3500$ K with $\mathcal{R} = 0$. As illustrated in Fig. 6, however, the residual can remain quite low along certain trajectories (black lines) in the domain defined by T_{vib} and T_{rot} coordinates. This results in large uncertainty. Where permissible due to signal-to-noise considerations, narrower spectrometer slit widths reduce the uncertainty and permit a more accurate determination of the vibrational and rotational temperatures. Note that under equilibrium conditions, the uncertainties are reduced because it is known that $T_{vib} = T_{rot} = T$ and the measurement is constrained.

The minimum residual between experiment and theoretical spectra is denoted $\mathcal{R}_{min}$ and corresponds to the best estimate of (T_{vib}, T_{rot}). We assume that our model perfectly accounts

for the experimental trends and that only Gaussian noise is present. The standard deviation of this Gaussian noise, σ, is estimated by taking the standard deviation over several camera pixels in regions where there is no signal. Given the residual defined in Eqn. 3, it is natural to then define a parameter $\mathcal{R}_m$:

$$\mathcal{R}_m = \frac{\sqrt{\sum_{\lambda_i} \delta_i^2}}{\sqrt{\sum_{\lambda_i} E(\lambda_i)^2}} \tag{4}$$

where δ_i denotes the normally distributed error with standard deviation σ at the pixel corresponding to wavelength λ_i. This provides an estimate of the minimum residual that would be achieved for a perfect fit in the presence of pure Gaussian noise. In fact, we find that the minimum residuals achieved are only slightly higher than this value. Thus, the assumption of white gaussian noise appears valid. In order to determine the uncertainty in the measurement, an estimate for residuals which correspond to a bad fit is needed. If indeed the error is well described by Gaussian noise and corresponds to a standard deviation σ then, for every pixel, 95% of the measured values will fall within $\pm 2\sigma$ of the true value. Given this, we define a cutoff value for the residual as:

$$\mathcal{R}_c = \frac{\sqrt{\sum_{\lambda_i} (2\sigma)^2}}{\sqrt{\sum_{\lambda_i} E(\lambda_i)^2}} = \frac{2\sigma\sqrt{\mathcal{N}}}{\sqrt{\sum_{\lambda_i} E(\lambda_i)^2}} \tag{5}$$

where $\mathcal{N}$ is the number of data points. This was used as the cutoff value between good and bad fits. All combinations of T_{vib} and T_{rot} for which $\mathcal{R} < \mathcal{R}_c$ were considered acceptable.

4. Results

4.1. Measurements at exit of plasma torch

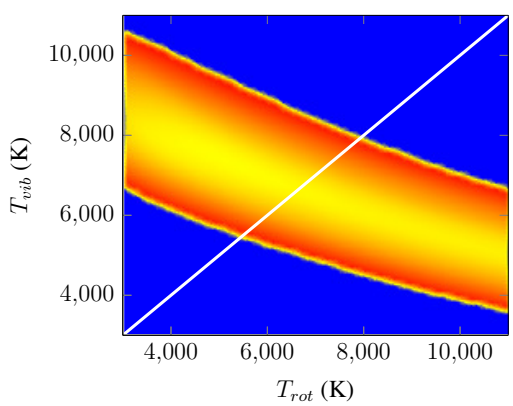

Figure 7. Residual of various fits to the experimental spectrum obtained at the torch exit. The color indicates the goodness of the fit: yellow corresponds to the best fits and red to the worse fits. Only the residuals of acceptable fits are shown: fits outside the acceptable window are colored blue. This contour surface represents the range of uncertainty in the measurement. The white line indicates the equilibrium coordinates $T_{vib} = T_{rot}$.

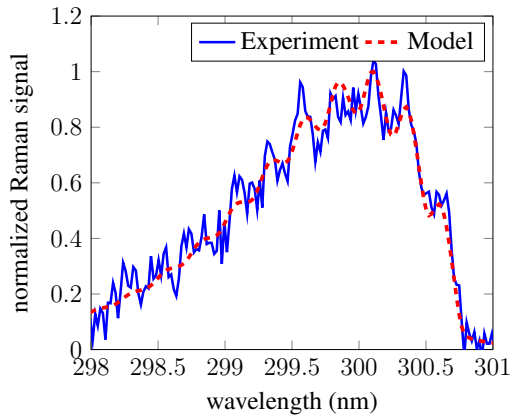

Figure 8. Best fit achieved under equilibrium assumption for $T_{vib} = T_{rot} = 6600$ K.

Raman measurements of temperature and density were first performed directly at the exit of the torch, which corresponds to the inlet of the water-cooled test section. The Raman measurements correspond to an average over a spatial window of approximately 4 mm centered on the nozzle axis. The high temperature and low gas density resulted in a relatively low signal-to-noise ratio for the measurement. This prohibited measurements from being made at the narrowest spectrometer slit width, which in turn reduced the sensitivity of the measurement to temperature. The residual contour shown in Fig. 7 illustrates the uncertainty in the measurement. Assuming equilibrium conditions ($T_{vib} = T_{rot}$), the best fit results in a temperature of 6600 ± 1000 K. This best fit is shown in Fig. 8. The measured temperature, along with Eqn. 2 and the corresponding Raman spectrum taken in room temperature air, can be used to estimate the density of molecular nitrogen. This yields a value of about $4.2(\pm 1.1) \times 10^{17}\, cm^{-3}$, corresponding to a nitrogen mole fraction of 0.38 ± 0.1. At a temperature of 6600 ± 1000 K, given the injection mixture of N_2 and Ar, the equilibrium density of N_2 corresponds to $4.0(\pm 3.5) \times 10^{17}\, cm^{-3}$. At a temperature of 6600 K, the equilibrium density corresponds to a mole fraction for molecular nitrogen of 0.36.

Spatially resolved measurements of temperature were also obtained by measuring the absolute emission of atomic nitrogen and argon lines. The measured temperature profiles are shown in Fig. 9 and are compared with the Raman measurements. To within the uncertainty of both measurements, they are in agreement with one another. Thus, despite the relatively large uncertainty in the Raman measurement, this confirms the assumption of thermal and chemical equilibrium at the torch exit.

4.2. Measurements at exit of water-cooled tube

Raman measurements of temperature and density were also first performed at the exit of the 15-cm water-cooled brass tube. As before, they correspond to an average over a spatial window of approximately 4 mm centered on the nozzle axis. Here, because the gas density is higher, the signal-to-noise was much better and a slit width of 100 μm (approximately 0.04 nm FWHM slit function) was used. This resulted in higher spectral resolution and an increased sensitivity to the

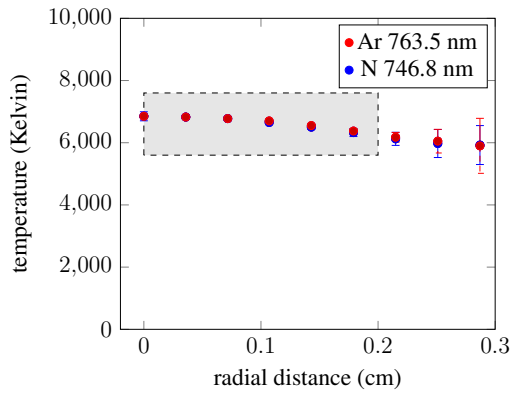

Figure 9. Temperature profile measured directly at the torch exit via absolute emission of the atomic N transition at 746 nm and the atomic Ar transition at 764 nm. The Raman spectroscopy measurement of temperature is represented by the highlighted grey region. The horizontal width of this grey box represents the spatial window over which the measurement was taken. The vertical height of the box represents the uncertainty in the Raman measurement. Note the extent of the radial axis: the nozzle perimeter is located at r = 0.5 cm.

vibrational and rotational temperatures.

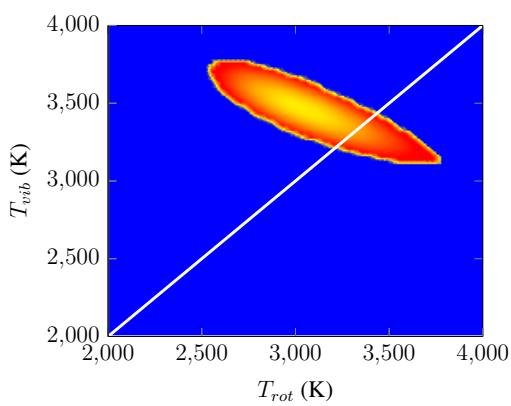

Figure 10. Residual of various fits to the experimental spectrum obtained at the exit of the water-cooled brass tube. The color indicates the goodness of the fit: yellow corresponds to the best fits and red to the worse fits. Only the residuals of acceptable fits are included: fits outside the acceptable window are colored blue. As with Fig. 7, this contour surface represents the range of uncertainty in the measurement. The best fit temperature was achieved for $T_{vib} = 2850$ K and $T_{rot} = 3850$ K. The white line indicates the equilibrium coordinates $T_{vib} = T_{rot}$.

As at the exit of the torch, the residual contour is centered on equilibrium temperature coordinates ($T_{vib} = T_{rot}$) suggesting that these degrees of freedom are equilibrated. If it is assumed that $T_{vib} = T_{rot}$, the best fit temperature occurs for $T = 3300 \pm 100$ K. The measured density is estimated at $1.4(\pm 0.3) \times 10^{18}\, cm^{-3}$, which corresponds to a mole fraction of 0.61 ± 0.1 at a temperature of 3300 K. At 3300 ± 100 K, the equilibrium nitrogen density is $1.43(\pm 0.05) \times 10^{18}\, cm^{-3}$. At 3300 K, the equilibrium mole fraction is 0.64. Note that atomic emission cannot be used for measurements of temperature at the exit of the 15-cm tube. Not

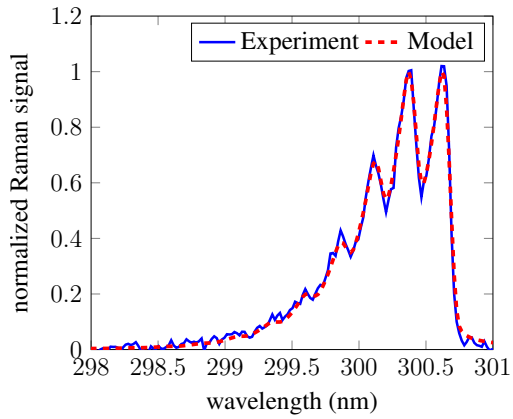

Figure 11. Best fit achieved between experimental spectra obtained at exit of water-cooled brass tube and the model corresponding to $T_{vib} = T_{rot} = 3300$ K.

only is the emission of atomic lines here too weak to measure, but these measurements rely on an assumption of full thermochemical equilibrium. The plasma at the exit of the 15-cm tube has been previously demonstrated to be out of equilibrium so that this approach is no longer valid.[8]

4.3. Rayleigh Scattering Measurements

A separate measure of temperature at the exit of the 15-cm water-cooled tube was desired for verification. For this, Rayleigh scattering was used to measure the total gas density. This total gas density, together with the known gas pressure of 1 atm, could be used to estimate the temperature via the gas equation of state. For a single temperature estimate, two Rayleigh scattering measurements were taken. The first one was taken at the exit of the 15-cm water-cooled tube. A second one was also taken at the exit of the 15-cm water-cooled tube but with the plasma torch turned off, providing a reference Rayleigh measurement at a temperature of 300 K in the N_2/Ar gas mixture. Given the known gas pressure of 1 atm, the ratio of these two measurements could be converted to a temperature estimate through the gas equation of state. The measurements were performed at the exact same location and under the same conditions as the Raman measurements at the exit of the 15-cm water-cooled tube. A laser wavelength of 281 nm was used and the laser was polarized vertically as with the Raman measurements. Scattered light was collected at a ninety degree collection angle from the laser propagation axis. The Rayleigh scattered signal was assumed to come solely from atomic argon and molecular nitrogen:

$$\mathcal{I}_{RL} = \eta V I_L n_0 \left(\mathcal{X}_{N2}\sigma_{N2} + \mathcal{X}_{Ar}\sigma_{Ar}\right) \tag{6}$$

where $\mathcal{I}_{RL}$ corresponds to the intensity of the Rayleigh scattered light, η represents a collection efficiency factor for the optical collection system, V represents the collection volume for Rayleigh scattering, I_L the intensity of the laser at the collection point and n_0 the total gas density at the collection point.[22] σ_{N2} and σ_{Ar} represent the right-angle Rayleigh scattering cross-section at the laser wavelength for molecular nitrogen and argon respectively. Note that the cross-sections σ_{N2} and σ_{Ar} are unknown at the laser wavelength. Limbach et al [23] report cross sections for various

species, including N_2, N, Ar as well as their respective ions, at a laser wavelength of 532 nm. The values for N, N^+ and Ar^+ are comparable to those of N_2 and Ar. Though we see strong evidence of chemical non-equilibrium as documented in Laux et al [8], the total densities of these species are still estimated to be significantly lower than those of N_2 and Ar under our conditions. Therefore, the assumption that the Rayleigh scattering signal comes solely from atomic argon and molecular nitrogen was viewed as reasonable. Furthermore, σ_{Ar} does not depend on the gas temperature and σ_{N2} changes by less than a few percent below 7000 K.[23]

If $\mathcal{I}_{Plasma}$ denotes the Rayleigh measurement with the torch ignited and $\mathcal{I}_{Ambient}$ denotes the Rayleigh measurement in the ambient gas mixture at 300 K, the ratio of these two signals yields:

$$\begin{aligned}\frac{\mathcal{I}_{Plasma}}{\mathcal{I}_{Ambient}} &= \frac{n_{Plasma}}{n_{Ambient}} \frac{(\mathcal{X}_{N2}\sigma_{N2} + \mathcal{X}_{Ar}\sigma_{Ar})_{Plasma}}{(\mathcal{X}_{N2}\sigma_{N2} + \mathcal{X}_{Ar}\sigma_{Ar})_{Ambient}} \\ &= \frac{T_{Ambient}}{T_{Plasma}} \frac{(\mathcal{X}_{N2}\sigma_{N2} + \mathcal{X}_{Ar}\sigma_{Ar})_{Plasma}}{(\mathcal{X}_{N2}\sigma_{N2} + \mathcal{X}_{Ar}\sigma_{Ar})_{Ambient}} \end{aligned} \tag{7}$$

where n_{Plasma} and $n_{Ambient}$ represent the total gas density with the torch ignited and in the ambient mixture, respectively. T_{Plasma} and $T_{Ambient}$ represent the temperature with the torch ignited and in the ambient mixture, respectively. The values in parentheses depend upon temperature and the subscripts '*Plasma*' and '*Ambient*' on these terms denote these values in the plasma and ambient mixture, respectively. The hypothesis that the chemical composition of the gas is approximately equal to that of the ambient mixture, and that the temperature dependence of the cross-section is negligible, removes any temperature dependence from the terms in parentheses in Eqn. 7. It follows that $\mathcal{I}_{Plasma}/\mathcal{I}_{Ambient} = T_{Ambient}/T_{Plasma}$.

For the measured Rayleigh scattered intensity, we integrated across the total line profile to obtain values for I_{Plasma} and $I_{Ambient}$. These measurements and the corresponding density estimates, yield a gas temperature estimate of 3100 ± 100 K. Because Rayleigh cross-section data is typically reported at 532 nm, the use of a 281 nm wavelength for Rayleigh scattering measurements was not an optimal choice. However, given our experimental configuration, this wavelength was more easily accessible and, furthermore, provided measurements in good agreement with the Raman measurements. As a verification step, similar measurements were done in the visible at the fundamental wavelength of the dye laser ($\lambda = 562$ nm). Here, the cross-sections for $\lambda = 532$ nm reported by Limbach et al [23] were used along with equilibrium mole fraction calculations for N, N_2 and Ar species as a function of temperature. This was done to account for any potentially significant variations in the Rayleigh cross-section or mole fractions. These calculations, when compared with the experimental data taken at $\lambda = 562$ nm, returned the same estimate of temperature.

5. Discussion

It is important to compare these new results with those of Gessman et al and Laux et al.[4, 5, 8] They report a measured temperature of 7200 ± 100 K at the water-cooled tube inlet. Our

measurements, from both emission using atomic nitrogen and argon and by the Raman scattering profile, indicate a slightly lower centerline temperature of about 6800 ± 100 K (Fig. 9). The slight discrepancy may be due to differences in the torch power or gas injection procedure used. Despite several attempts, we were not able to operate using the same gas injection scheme. However, the emission measurements show that the two conditions are reasonably close.

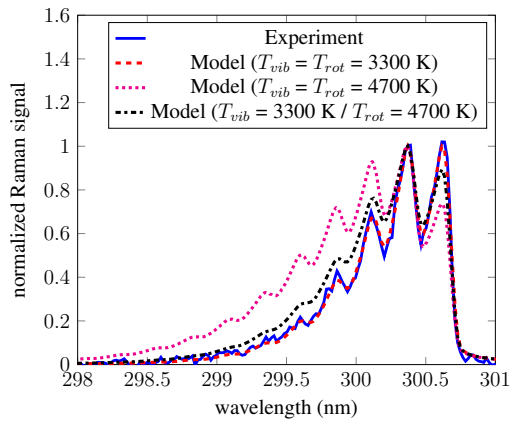

Figure 12. Same spectra as shown in Figure 11 but with a theoretical spectrum calculated for $T_{vib} = T_{rot} = 4700$ K and a theoretical spectrum calculated for $T_{vib} = 3300$ K / $T_{rot} = 4700$ K added for comparison. All plots are normalized to their maximum value.

At the exit of the 15-cm water-cooled brass tube, Laux et al [6] report rotational temperature measurements of 4715 $\pm$ 100 K. These were measured by fitting rotational lines of the N_2^+ first negative system. We repeated these emission measurements and found essentially the same results. Namely, we obtained a comparable estimate of the rotational temperature and observed similar non-equilibrium distributions in the N_2 B and C electronic states as reported in Refs. [4, 5, 8]. This served as another indicator that, while the operating conditions used were slightly different than those of Gessman et al and Laux et al., the essential characteristics of their experiment were reproduced. The Raman measurements presented in this paper offer a new perspective on this recombining plasma by targeting the nitrogen ground state. They supply a measure of the vibrational temperature, previously unavailable by emission measurements, in addition to measures of rotational temperature and density. These results show that $T_{vib} = T_{rot} = 3300 \pm 100$ K. Figure 12 shows a comparison between the measured Raman spectrum, a theoretical Raman spectrum calculated for $T_{vib} = T_{rot} = 3300$ K, a theoretical Raman spectrum calculated for $T_{vib} = T_{rot} = 4700$ K and a theoretical Raman spectrum calculated for $T_{vib} = 3300$ K / $T_{rot} = 4700$ K to illustrate that a temperature of 4700 K cannot be explained by the experimental Raman measurements.

While the Rayleigh scattering measurements support the Raman measurements, the discrepancy between the emission measurements remains. Such discrepancies can arise when production and/or decay mechanisms are faster than rotational-translational relaxation.[24] While the Raman measurements show that $T_{vib} = T_{rot}$, the measured distributions of the N_2 B and C states observed via emission spectroscopy suggest that these electronic and vibrational levels do

not follow a Boltzmann distribution.[4, 5, 8] Furthermore, the electron density, measured via Stark-broadened hydrogen emission in Ref [5], is much higher than the equilibrium values for both 4700 K and 3300 K. It was also shown in Ref. [5] that there is a significant overpopulation of N atoms at the exit of the 15-cm water-cooled tube. Any of these observed non-equilibrium phenomena could potentially perturb the rotational temperature measurements made via emission spectroscopy of the N_2^+ ion. Bruggeman et al [24] give examples of scenarios in which optical emission spectroscopic measurements yield incorrect estimates of the gas rotational temperature. Studer and Vervisch report similar discrepancies in rotational temperature between emission measurements of the first negative system and Raman measurements. They argue that, as a recombining plasma, excited species such as $B\,^2\Sigma_u^+$ state of N_2^+ that are produced via chemical reactions are rapidly depopulated and do not have time to equilibrate to the background rotational temperature of the gas.[17]

6. Conclusion

To summarize, we presented ultraviolet Raman scattering measurements in a recombining plasma. The measurements permit direct interrogation of the molecular nitrogen ground state and supply measurements of density, rotational temperature and vibrational temperature. Raman scattering measurements made directly at the inlet of the water-cooled tube are in agreement with atomic emission measurements of temperature and confirm that the plasma is at equilibrium with a temperature of approximately 6800 K. Measurements performed at the exit of a 15-cm water-cooled tube used to rapidly cool the plasma and produce non-equilibrium distributions, show that both the vibrational and rotational temperatures are equal to about 3300 K, i.e. much lower than measurements of rotational temperature made by emission spectroscopy using the first negative system of N_2^+. Future work aims to study the recombining plasma in more detail and to understand the discrepancy between the results from Raman scattering measurements and from emission spectroscopy measurements. Understanding non-equilibrium radiating plasmas is important for atmospheric entry applications, particularly for afterbody heat transfer and plasma processing.

Acknowledgments

This work was supported through a Centre National d'Études Spatiales (CNES) postdoctoral fellowship (technical monitor: Julien Annaloro). Augustin Tibère-Inglesse was supported by CIFRE grant number 42701092/20160218/JSE with Airbus Safran Launchers (technical monitor: Laurent Visconti).

References

[1] C.O. Johnston and A.M. Brandis. Features of afterbody radiative heating for earth entry. *Journal of Spacecraft and Rockets*, 52(1):105–119, 2014.

[2] C.O. Johnston and M. Panesi. Advancements in afterbody radiative heating simulations for earth entry. In *46th AIAA Thermophysics Conference*, 2016.

[3] C.O. Laux. *Optical Diagnostics and Radiative Emission of Air Plasmas*. PhD thesis, Stanford University, Dept. of Mechanical Engineering, 1993.

[4] R.J. Gessman, C.O. Laux, and C.H. Kruger. Experimental study of kinetic mechanisms of recombining atmospheric pressure air plasmas. In *28th Plasmadynamics and Lasers Conference*, number AIAA-1997-2364. American Institute of Aeronautics and Astronautics, 1997.

[5] R.J. Gessman. *An Experimental Investigation of the Effects of Chemical and Ionizational Nonequilibrium in Recombining Atmospheric Pressure Air Plasmas*. PhD thesis, Stanford University, 2000.

[6] C.O. Laux, R.J. Gessman, C.H. Kruger, F. Roux, F. Michaud, and S.P. Davis. Rotational temperature measurements in air and nitrogen plasmas using the first negative system of N_2^+. *Journal of Quantitative Spectroscopy and Radiative Transfer*, 68(4):473 – 482, 2001.

[7] C.O. Laux, T.G. Spence, C.H. Kruger, and R.N. Zare. Optical diagnostics of atmospheric pressure air plasmas. *Plasma Sources Science and Technology*, 12(2):125, 2003.

[8] C.O. Laux, L. Pierrot, and R.J. Gessman. State-to-state modeling of a recombining nitrogen plasma experiment. *Chemical Physics*, 398:46 – 55, 2012.

[9] A.C. Eckbreth. Laser diagnostics for combustion temperature and species. In *Combustion Science & Technology Book Series*. Gordon and Breach, 2nd edition, 1996.

[10] A. Roettgen, W. Lempert, and I. Adamovich. Measurements of N_2 vibrational distribution function in pulsed nanosecond nonequilibrium discharge by spontaneous Raman scattering. In *51st AIAA Aerospace Sciences Meeting including the New Horizons Forum and Aerospace Exposition*, number AIAA-2013-0576. American Institute of Aeronautics and Astronautics, 2013.

[11] A. Lo, G. Cléon, P. Vervisch, and A. Cessou. Spontaneous Raman scattering: a useful tool for investigating the afterglow of nanosecond scale discharges in air. *Applied Physics B*, 107(1):229–242, 2012.

[12] A Lo, A Cessou, P Boubert, and P Vervisch. Space and time analysis of the nanosecond scale discharges in atmospheric pressure air: I. Gas temperature and vibrational distribution function of N_2 and O_2. *Journal of Physics D: Applied Physics*, 47(11):115201, 2014.

[13] Walter R. Lempert and Igor V. Adamovich. Coherent anti-Stokes Raman scattering and spontaneous Raman scattering diagnostics of nonequilibrium plasmas and flows. *Journal of Physics D: Applied Physics*, 47(43):433001, 2014.

[14] S.P. Sharma, S.M. Ruffin, W.D. Gillespie, and S.A. Meyer. Vibrational relaxation measurements in an expanding flow using spontaneous Raman scattering. *Journal of Thermophysics and Heat Transfer*, 7(4):697–703, 2017/03/09 1993.

[15] H. Pilverdier, R. Brun, and M. P. Dumitrescu. Emission and Raman spectroscopy measurements in hypersonic nitrogen flows. *Journal of Thermophysics and Heat Transfer*, 15(4):484–490, 2001.

[16] John Gilmore, Surendra Sharma, Douglas Fletcher, and Daniel Bershader. Single-pulse spontaneous Raman scattering measurements in an expanding nitrogen/oxygen admixture. In *30th Thermophysics Conference*. American Institute of Aeronautics and Astronautics, 2017/09/06 1995.

[17] Damien Studer and Pierre Vervisch. Raman scattering measurements within a flat plate boundary layer in an inductively coupled plasma wind tunnel. *Journal of Applied Physics*, 102(3):033303, 2007.

[18] M. MacDonald and C.O. Laux. Experimental characterization of ablation species in an air plasma ablating boundary layer. In *11th AIAA/ASME Joint Thermophysics and Heat Transfer Conference*, number AIAA-2014-2251. American Institute of Aeronautics and Astronautics, June 2014.

[19] M. E. MacDonald, C. M. Jacobs, and C. O. Laux. Interaction of air plasma with ablating heat shield material. *IEEE Transactions on Plasma Science*, 42(10):2658–2659, Oct 2014.

[20] M.E. MacDonald, C.M. Jacobs, C.O. Laux, F. Zander, and R.G. Morgan. Measurements of air plasma/ablator interactions in an inductively coupled plasma torch. *Journal of Thermophysics and Heat Transfer*, 29(1):12–23, 2014.

[21] B. J. McBride and S. Gordon. Computer program for calculating and fitting thermodynamic functions. Technical report, NASA RP-1271, 1992.

[22] R.B. Miles, W.R. Lempert, and J.N. Forkey. Laser rayleigh scattering. *Measurement Science and Technology*, 12(5), 2001.

[23] C. Limbach, C. Dumitrache, and A.P. Yalin. Laser light scattering from equilibrium, high temperature gases: limitations on Rayleigh scattering thermometry. In *47th AIAA Plasmadynamics and Lasers Conference*, number AIAA 2016-3381. American Institute of Aeronautics and Astronautics, 2016.

[24] P.J. Bruggeman, N. Sadeghi, D.C. Schram, and V. Linss. Gas temperature determination from rotational lines in non-equilibrium plasmas: a review. *Plasma Sources Science and Technology*, 23(2):023001, 2014.